Modeling and Analysis of Bridge-Leg Crosstalk of GaN HEMT Considering Nonlinear Junction Capacitances

Binxing Li, *Student Member, IEEE*, Gaolin Wang, *Senior Member, IEEE*, Shaobo Liu, Nannan Zhao, *Member, IEEE*, Guoqiang Zhang, *Member, IEEE*, Xueguang Zhang, *Member, IEEE*, and Dianguo Xu, *Fellow, IEEE*

***Abstract*—Gallium nitride high electron mobility transistor (GaN HEMT) has fast switching speed and low threshold voltage, which could result in a severe false triggering voltage pulse at the synchronous freewheeling transistor in bridge-leg circuit when the control transistor turns ON. To suppress the crosstalk phenomenon, this article proposes an analytical model about the crosstalk voltage, with consideration of nonlinearities in capacitance–voltage (*C–V*) of GaN HEMT. By utilizing the equivalent circuit of control transistor and synchronous freewheeling transistor, the number of analytical model parameters to be extracted can be reduced significantly. Besides, the nonlinear characteristic of junction capacitances is taken into account in the model, and the accuracy is verified by the current–voltage (*I–V*) curve of capacitances. Based on the model, an exhaustive investigation into the impact of device and circuit parameters on the crosstalk phenomenon is conducted. Further, for the purpose of evaluating the oscillation of crosstalk voltage, the damping ratio and oscillation frequency are acquired. The proposed model can be applied to guiding GaN device selection and printed circuit board (PCB) circuit design. The effectiveness and superiority of the proposed model are verified with simulations and experiments on a double pulse test platform.**

***Index Terms*—Analytical model, bridge-leg configuration, crosstalk phenomenon, gallium nitride high electron mobility transistor (GaN HEMT).**

I. Introduction

In recent years, the third-generation semiconductor power electronic devices represented by gallium nitride (GaN) and silicon carbide (SiC) devices have received increasing attention from the academic and industrial communities. Compared with silicon-based semiconductor devices, wide band gap devices have shown great advantages and potentials in terms of switching speed, operating frequency, and energy efficiency [1]–[7]. In particular, the reverse recovery loss of GaN devices is zero, which makes them suitable for bridge topologies [8]. Although GaN power devices have many advantages, due to the short development time and immature technology, there are still many challenges in applications. Taking gallium nitride high electron mobility transistor (GaN HEMT) as an example, the device has poor breakdown resistance and short-circuit characteristics. The reverse conduction voltage drop is relatively large, and the safe operating range is relatively limited. In addition, the high *dv/dt* problem caused by the high switching speed of GaN devices amplifies the impact of parasitic parameters on drive reliability significantly [9]–[15].

Bridge-leg modules are found in many power converter configurations, including synchronous buck converters, inverters, and many other bridge-based topologies. In the bridge-leg circuit, when the control transistor (CtrlTR) turns ON, the drain–source voltage of synchronous freewheeling transistor (SyncTR) increases to dc-link voltage sharply. Meanwhile, a false triggering pulse at the gate of SyncTR will appear, which is called crosstalk voltage. When the crosstalk voltage exceeds the threshold voltage, the SyncTR will falsely turn ON. The false turn-ON phenomenon on Si-based bridge-leg circuit has been investigated in detail [16]–[20]. When the drain–source voltage of CtrlTR decreases, the voltage on SyncTR will increase. At this time, the displacement current of SyncTR flowing through gate–drain capacitance charges gate–source capacitance and flows through the drive circuit meanwhile. The impedance of the drive circuit has an appreciable effect on crosstalk voltage [16]. Thus, reducing the drive circuit impedance and increasing the gate–source capacitance additionally could suppress crosstalk voltage [19], [20]. Nevertheless, the method may not be suitable for the bridge-leg configuration that two active switches take turns to be the control and the synchronous switches, depending on the direction of the load current. Active miller clamping is also an effective method to suppress the crosstalk voltage. In [21], the active miller clamping circuit was used to bypass the drive circuit impedance in a half-bridge circuit based on IGBT. The active miller clamping circuit was also added to keep MOSFET turned OFF reliably [22]. However, it needs additional drive signals. To select appropriate circuit parameters, analytical

Manuscript received March 27, 2020; revised July 10, 2020; accepted September 8, 2020. Date of publication September 18, 2020; date of current version November 20, 2020. This work was supported in part by the Research Fund for the National Natural Science Foundation of China under Grants 51961130385, 51877054, and 51807037, and in part by the Power Electronics Science and Education Development Program of Delta Group under Grant DREM2018001. Recommended for publication by Associate Editor A. Mertens. (*Corresponding author: Gaolin Wang.)*

The authors are with the Department of Electrical Engineering, School of Electrical Engineering and Automation, Harbin Institute of Technology, Harbin 150001, China (e-mail: li_binxing@163.com; wgl818@hit.edu.cn; liushaobo-hit@163.com; znn429@126.com; zhgq@hit.edu.cn; zxghit@hit.edu.cn; xudiang@hit.edu.cn).

Color versions of one or more of the figures in this article are available online at https://ieeexplore.ieee.org.

Digital Object Identifier 10.1109/TPEL.2020.3024962

model based bridge-leg configuration was established [17], [18]. In [17], the displacement current of CtrlTR and body diode were taken into account in the model, based on which, the effects of them on crosstalk voltage were analyzed. The nonlinear junction capacitances need considering to improve the model accuracy. In [18], the influence of the common source inductance shared by power and drive circuits was analyzed based on the analytical model, which considered the nonlinear gate–drain capacitance. However, the oscillation characteristic of crosstalk voltage was ignored.

Compared with Si-based devices, there is no body diode in GaN devices and the input capacitance is only one-tenth of the Si-based device but the output capacitance and reverse transfer capacitance in GaN devices are close to the MOSFET at the same power level [23], [24]. According to the previous study in [16], [17], and [25], the crosstalk voltage pulse magnitude will increase with the increase of $C_{\rm gd}$ and the decrease of $C_{\rm gs}$, and the $C_{\rm oss}$ has little effect on the crosstalk voltage. Therefore, the danger of crosstalk in GaN devices is more serious than Si-based MOSFET. Besides, the GaN device is more sensitive to the crosstalk voltage because the threshold voltage of the GaN device is low. Hence the effects of circuit parameters on crosstalk voltage could be more complicated. In previous work, PSpice model and analytical model of bridge-leg configuration are the most commonly used methods for switching behavior or crosstalk analysis [15], [26]–[29]. PSpice models have a higher precision, which can get a more accurate crosstalk voltage after obtaining the accurate circuit parameters. However, according to the PSpice model, the real crosstalk voltage inside the device package is difficult to be obtained. It is not conducive to analyzing the influence of circuit parameters on crosstalk oscillation, especially the attenuation speed.

In the analytical models, a full parameter analytical model, which contains all the parasitic parameters of CtrlTR and SyncTR can get a more accurate crosstalk voltage transient waveform [26]. The influence of various device and circuit parameters could be analyzed, and an appropriate circuit design for false turn-ON mitigation was provided. However, the model is relatively complicated and many model parameters need to be extracted and adjusted. In [27], a simplified analytical model was established focusing on the SyncTR. The CtrlTR was equivalent to a slope power supply, which could reduce the complexity of the model and improve the simulation efficiency. However, the nonlinearity of junction capacitances was not considered in the model, which may result in the reduced model accuracy.

This article proposes a crosstalk voltage analytical model for bridge-leg circuit considering the nonlinear junction capacitances of the GaN device to adjust the amplitude and oscillation of the crosstalk voltage. The model is conductive to guiding GaN device selection and printed circuit board (PCB) circuit design for suppressing the crosstalk voltage. Different from the PSpice circuit models and other equation analytical models, a method of circuit equivalence and iterative solution of nonlinearity is adopted to reduce the complexity of the model. Meanwhile, the damping ratio and oscillation frequency of crosstalk voltage can be calculated easily. The attenuation characteristic of crosstalk voltage can be analyzed according to damping ratio and the oscillation frequency. The transient values of the crosstalk voltage can be calculated accurately in every iteration. In addition, the influences of circuit parameters on the crosstalk voltage amplitude and oscillation characteristics of the freewheeling transistor are analyzed effectively. Such as the power circuit stray inductance, the gate resistance, the drive circuit inductance, and the common source inductance. The proposed model and analysis results are verified with simulations and experiments on a double pulse test (DPT) platform.

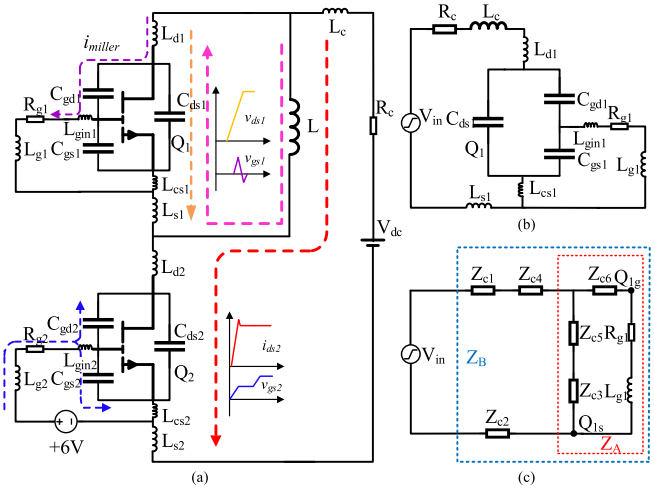

Fig. 1. Bridge-leg configuration and equivalent circuits in crosstalk process. (a) Equivalent circuit of the GaN-based bridge-leg configuration with inductance load. (b) Equivalent circuit in crosstalk process. (c) Simplified circuit.

The rest of this article is organized as follows. The analytical model of bridge-leg crosstalk voltage with constant capacitances is first introduced. Then the nonlinear junction capacitances are modeled and the proposed analytical model considered nonlinear junction capacitances are established in Section II. In Section III, the influences of the device and circuit parameters on crosstalk voltage are analyzed based on the simulation. The test and experiment results are presented in Section IV to verify the model and theoretical analysis. Finally, Section V concludes the article.

II. Analytical Modeling of Bridge-Leg Crosstalk

A. Analytical Model of Crosstalk With Constant Capacitances

Fig. 1(a) shows the equivalent circuit of the GaN-based bridge-leg configuration with inductance load. Q_2 can be seen as the CtrlTR and Q_1 is the SyncTR. The parasitic parameters of GaN HEMTs, the equivalent resistances and inductances of circuits are also shown, since they have an obvious influence on the gate voltage of SyncTR. In the circuit, $C_{\rm gdn}$, $C_{\rm gsn}$, and $C_{\rm dsn}$ are the junction capacitances. $L_{\rm dn}$, $L_{\rm sn}$, and $L_{\rm ginn}$ are the electrode parasitic inductances of the package. $L_{\rm csn}$ is the common source inductance shared by the power circuit and drive circuit. $R_{\rm gn}$ and $L_{\rm gn}$ are the main impedances of drive circuit, where $n = 1, 2$. $L_{\rm c}$ and $R_{\rm c}$ represent the equivalent stray inductance and resistance of power circuit, respectively. L is the load inductance.

When Q_2 turns ON, the load current path transforms from Q_1 [pink line in Fig. 1(a)] to Q_2 [red line in Fig. 1(a)]. After CtrlTR takes all the load current, the drive current still flows toward the gate terminal of CtrlTR, which leads to the decrease of drain–source voltage. The dc-link voltage $V_{\rm dc}$ is fixed, therefore the drain–source voltage of SyncTR increases rapidly. At the same time the junction capacitances $C_{\rm ds1}$ and $C_{\rm gd1}$ of SyncTR will be charged [orange line in Fig. 1(a)]. The displacement current charging $C_{\rm gd1}$ [i.e., $i_{\rm miller}$ in Fig. 1(a)] flows through the drive circuit of SyncTR, resulting in an unexpected triggering voltage pulse at the gate terminal of SyncTR. The turn-ON of CtrlTR is the fundamental reason for crosstalk. In order to simplify the model and reduce simulation time, the CtrlTR in bridge circuit is equaled as a voltage source $V_{\rm ctrl}$, which can be represented as

$$V_{\rm ctrl} = \begin{cases} V_{\rm dc} - \frac{V_{\rm dc}}{T_{\rm f}} & 0 < t < T_{\rm f} \\ 0 & T_{\rm f} < t \end{cases} \tag{1}$$

where $V_{\rm dc}$ and $T_{\rm f}$ are the dc-link voltage and $V_{\rm ctrl}$ fall time, respectively.

In Fig. 1(a), according to Kirchhoff's law, the dc source $V_{\rm dc}$ and $V_{\rm ctrl}$ series can be seen as the input voltage $V_{\rm in}$ shown in Fig. 1(b) for studying the characteristics of crosstalk in bridge-leg circuit based GaN HEMT. $V_{\rm in}$ can be expressed as

$$V_{\rm in} = \begin{cases} \frac{V_{\rm dc}}{T_{\rm f}} t & 0 < t < T_{\rm f} \\ V_{\rm dc} & T_{\rm f} < t. \end{cases} \tag{2}$$

As shown in Fig. 1(b), the crosstalk voltage $V_{\rm gs}$ can be regarded as a response to the input voltage $V_{\rm in}$. The relationship between $V_{\rm gs}$ and $V_{\rm in}$ demonstrates the essential characteristics of the crosstalk phenomenon. In order to investigate this behavior, the structure can be simplified as shown in Fig. 1(c), where the impedances $Z_{\rm c1}$, $Z_{\rm c2}$, and $Z_{\rm c3}$ are determined as

$$Z_{\rm c1} = R_{\rm c} + sL_{\rm c} + sL_{\rm d1} \tag{3}$$

$$Z_{\rm c2} = sL_{\rm s1} \tag{4}$$

$$Z_{\rm c3} = sL_{\rm cs1}. \tag{5}$$

$C_{\rm gd1}$, $C_{\rm gs1,}$ and $C_{\rm ds1}$ form a delta connection in Fig. 1(b), which can be changed into a star connection by using the following formulas

$$Z_{\rm c4} = \frac{\frac{1}{sC_{\rm ds1}} \cdot \frac{1}{sC_{\rm gd1}}}{\frac{1}{sC_{\rm ds1}} + \frac{1}{sC_{\rm gd1}} + \frac{1}{sC_{\rm gs1}}} \tag{6}$$

$$Z_{\rm c5} = \frac{\frac{1}{sC_{\rm ds1}} \cdot \frac{1}{sC_{\rm gs1}}}{\frac{1}{sC_{\rm ds1}} + \frac{1}{sC_{\rm gd1}} + \frac{1}{sC_{\rm gs1}}} \tag{7}$$

$$Z_{\rm c6} = \frac{\frac{1}{sC_{\rm gs1}} \cdot \frac{1}{sC_{\rm gd1}}}{\frac{1}{sC_{\rm ds1}} + \frac{1}{sC_{\rm gd1}} + \frac{1}{sC_{\rm gs1}}} + sL_{\rm gin1} \tag{8}$$

where $Z_{\rm c4}$, $Z_{\rm c5}$, and $Z_{\rm c6}$ are the calculated impedances of star connections, as shown in Fig. 1(c).

The impedance $Z_{\rm A}$ of the two parallel branches shown in Fig. 1(c) can be described as

$$Z_{\rm A} = \frac{(Z_{\rm c6} + R_{\rm g1} + sL_{\rm g1}) \cdot (Z_{\rm c5} + Z_{\rm c3})}{Z_{\rm c6} + R_{\rm g1} + sL_{\rm g1} + Z_{\rm c5} + Z_{\rm c3}}. \tag{9}$$

TABLE I
DEVICE AND CIRCUIT PARAMETERS

Symbol	Parameter	Value
$L_{\rm c}$	Power circuit stray inductance (nH)	39
$L_{\rm dn}$	Drain inductance (nH)	0.45
$L_{\rm sn}$	Source inductance (nH)	0.084
$L_{\rm csn}$	Common source inductance (nH)	0.4
$L_{\rm ginn}$	Gate internal inductance (nH)	0.65
$L_{\rm gn}$	Drive circuit inductance (nH)	5
$R_{\rm c}$	Power circuit resistance (mΩ)	4.5
$R_{\rm gn}$	Gate resistance (Ω)	4

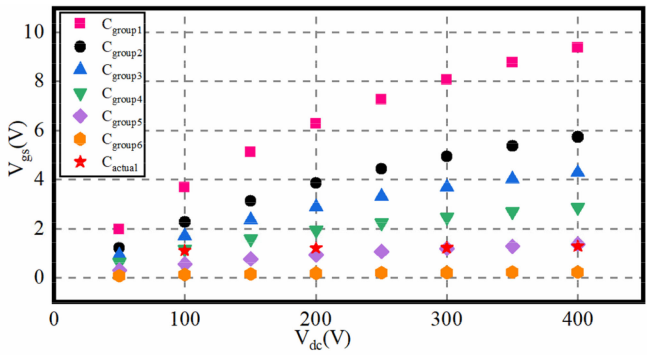

Fig. 2. Comparison of fixed junction capacitances crosstalk model simulation results and experimental results.

Then the total impedance of the circuit $Z_{\rm B}$ can be obtained as

$$Z_{\rm B} = Z_{\rm c1} + Z_{\rm c4} + Z_{\rm A} + Z_{\rm c2}. \tag{10}$$

Therefore, the crosstalk voltage between gate and source can be calculated by Kirchhoff's law from the input voltage $V_{\rm in}$. The complex frequency domain model of crosstalk voltage can be expressed as

$$G(s) = \frac{V_{\rm gs}(s)}{V_{\rm in}(s)} = \frac{Z_{\rm A}}{Z_{\rm B}} \cdot \frac{R_{\rm g1} + sL_{\rm g1}}{Z_{\rm c6} + R_{\rm g1} + sL_{\rm g1}}. \tag{11}$$

It is convenient to analyze the influence of circuit parameters on crosstalk voltage using (11). The time-domain expression of $V_{\rm gs}$ can be obtained according to (11) through Laplace inverse transformation to investigate the amplitude and the oscillation of crosstalk voltage. The values of parameters employed in the subsequent analysis are in accordance with the parameters of the experimental prototype in Section IV, as listed in Table I.

However, the actual process of generating crosstalk phenomenon is more complicated, especially the variation of the power device parasitic elements. According to the GaN device datasheet, the junction capacitances especially $C_{\rm gd}$ and $C_{\rm ds}$ are not constant when the drain–source voltage changes. In order to investigate the influence of capacitances variation, the capacitances values under 0–50 V with 10 V interval from datasheet are used as model parameters. They are denoted as $C_{\rm group1}$–$C_{\rm group6}$ and the amplitude of the crosstalk voltage $V_{\rm gs}$ is simulated using the model in Section II-A. The ramp ratio of $V_{\rm in}$ is 40 V/ns close to the actual slope. The simulation and experimental results ($C_{\rm actual}$) are shown in Fig. 2. It shows that the errors between simulation results of the fixed capacitance model and experimental results change with the drain–source

TABLE II
PARAMETERS OF NONLINEAR CAPACITANCE MODELS

	Parameters	Range of Drain-Source Voltage
Output Capacitance C_{oss}(pF)	$C_0 = 455.1$ $C_m = 45.88$ $C_n = 0$	V_{ds}<0V
	$C_0 = 455.1$ $C_m = 45.88$ $C_n = -0.106$	0V≤V_{ds}<25V
	$C_0 = 65.9$ $C_m = 565.4$ $C_n = -0.0175$	25V≤V_{ds}<400V
	$C_0 = 65.9$ $C_m = 0.5$ $C_n = 0$	V_{ds}≥400V
Reverse Transfer Capacitance C_{rss}(pF)	$a_0 = 62.4$ $a_j = 0$, j = 1, 2, … ,6	V_{ds}<0V
	$a_0 = 58.9$ $a_1 = -3.88$ $a_j = 0$, j = 2, 3, … ,6	0V≤V_{ds}<4.7V
	$a_0 = 44.896$ $a_1 = -0.894$ $a_j = 0$, j = 2, 3, … ,6	4.7V≤V_{ds}<48V
	$a_0 = 3.8789$ $a_1 = -0.07182$ $a_2 = 8.681\times10^{-4}$ $a_3 = -5.438\times10^{-6}$ $a_4 = 1.771\times10^{-8}$ $a_5 = -2.808\times10^{-11}$ $a_6 = 1.713\times10^{-14}$	48V≤V_{ds}<400V
	$a_0 = 1.927$ $a_j = 0$, j = 1, 2, … ,6	V_{ds}≥400V

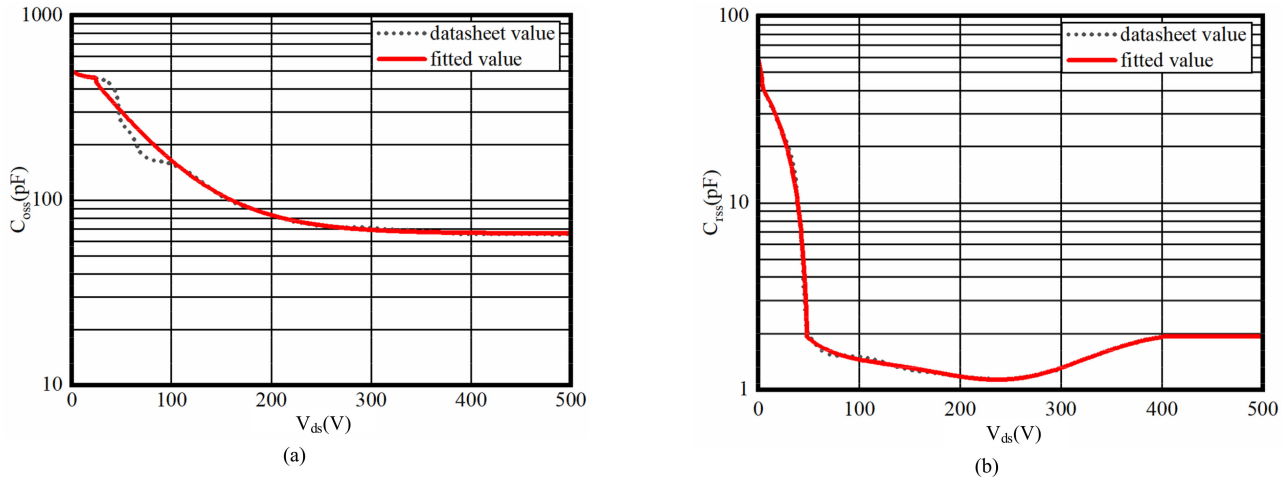

Fig. 3. Comparisons between fitted results and datasheet. (a) Output capacitance. (b) Reverse transfer capacitance.

voltage. Hence it cannot adapt to different operating voltage conditions. In the actual process, the junction capacitances vary with voltage whereas they are regarded as constant in the model. Therefore, in order to improve the accuracy of the crosstalk voltage in the circuit, the influence of the junction capacitances nonlinearity can no longer be ignored.

B. Modeling for Nonlinear Junction Capacitances

The dynamic characteristics of GaN HEMT crosstalk voltage are mainly influenced by three junction capacitances [30],[31]. According to the capacitance–voltage (C–V) characteristic curves provided in the datasheet, the gate–source capacitance C_{gs}, the gate–drain capacitance C_{gd}, and the drain–source capacitance C_{ds} can be described with the voltage-dependent nonlinear equations [28], [29].

With the help of data extraction software GetData, data information of the input capacitance C_{iss}, the output capacitance C_{oss}, and the reverse transfer capacitance C_{rss} of GS66508B (GaN device produced by GaN Systems. Inc) can be converted from the C–V characteristic curves. According to the curves, the equation of C_{oss} and C_{rss} can be obtained by fitting. It should be noted that C_{iss} hardly changes with voltage. In order to decrease the complexity, it can be regarded as constant value. The equations of C_{oss} and C_{rss} can be obtained as follows

$$C_{oss} = C_0 - C_m e^{C_n V_{ds}} \tag{12}$$

$$C_{rss} = a_0 + a_1 V_{ds} + a_2 V_{ds}^2 + a_3 V_{ds}^3 + a_4 V_{ds}^4 + a_5 V_{ds}^5 + a_6 V_{ds}^6 \tag{13}$$

where C_0, C_m, C_n, and a_0–a_6 are related parameters of the nonlinear capacitance models. The values of them have been obtained by data fitting software Origin and shown as Table II.

According to the parameters presented in Table II, the model of nonlinear capacitances can be established. Then the result curves can be obtained by calculating and plotting. Fig. 3 shows the comparisons between fitted curves (solid lines) and datasheet curves (dashed lines) of C_{oss} and C_{rss}, respectively. The fitted curves are in good agreement with datasheet curves.

Due to the relationship among the output capacitance, the reverse transfer capacitance and the junction capacitances (C_{gd} and C_{ds}), i.e., $C_{gd} = C_{rss}$ and $C_{ds} = C_{oss} - C_{rss}$, the model of junction capacitances can be obtained. The accuracy of junction

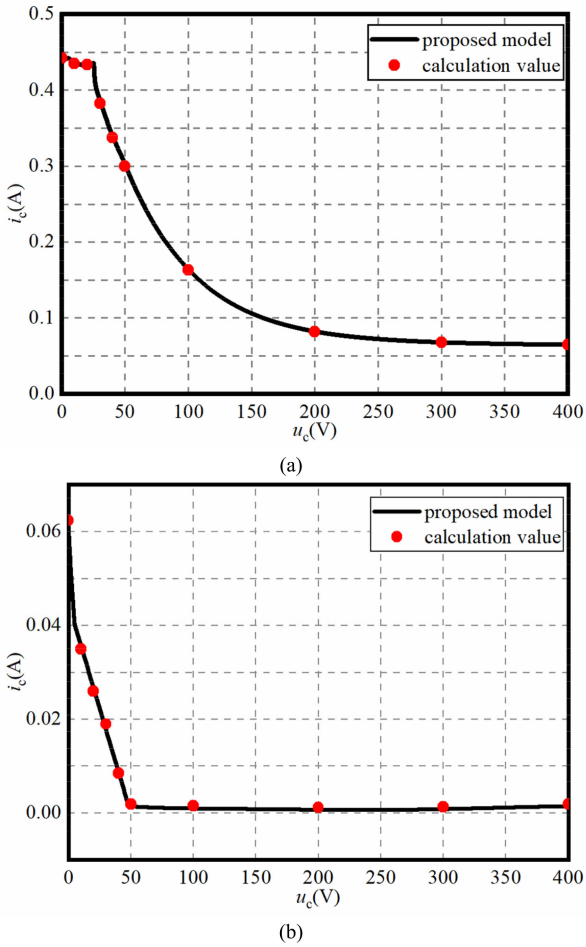

Fig. 4. Comparisons between current simulation results and calculation results based on datasheet. (a) Drain–source capacitance. (b) Gate–drain capacitance.

capacitance model is able to be verified by comparing the capacitance current simulation curves with calculated results based on datasheet. The current–voltage curves can be obtained with the time domain transient simulation under different voltage with the same ramp ratio. Fig. 4 shows the comparisons between simulation curves (solid lines) and calculation result curves (discrete points) of $C_{\rm ds}$ and $C_{\rm gd}$, respectively. The simulation curves are in good agreement with calculation results, which verified the accuracy of junction capacitance model.

C. Analytical Model of Crosstalk With Nonlinear Capacitances

For the analytical crosstalk model containing nonlinear elements, the relationship between the crosstalk voltage $V_{\rm gs}$ and $V_{\rm in}$ cannot be obtained as a transfer function like constant capacitance crosstalk model in Part A. Then, the circuit model [26] or the PSpice model [29] can be established. In this article, the crosstalk voltage generated by the circuits containing nonlinear elements can be divided into a great number of computing period. In each period, the capacitance is a constant, and the model is a linear model. However, the initial values of the system are not zero yet, which are determined by the previous period. The equivalent circuit model in Fig. 1(c) can be converted to

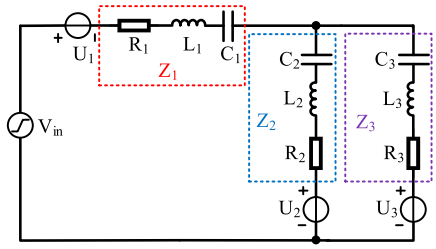

Fig. 5. *RLC* equivalent circuit of the bridge-leg configuration in crosstalk process.

Fig. 5, considering the initial currents of inductances and the voltages of capacitances. In Fig. 5, $U_{\rm n}$, $R_{\rm n}$, $L_{\rm n}$, and $C_{\rm n}$ are the initial voltage, resistance, inductance, and capacitance of branch n, respectively, where $n = 1$, 2, and 3. The relationship among the equivalent circuit parameters can be expressed as

$$\begin{cases} L_1 = L_{\rm c} + L_{\rm d1} + L_{\rm s1} \\ C_1({\rm k}) = \frac{Z_4({\rm k})}{s} \\ R_1 = R_{\rm c} \\ U_1 = \frac{U_{\rm C1}(k-1)}{s} - L_1 I_{\rm L1}(k-1) \end{cases} \tag{14}$$

$$\begin{cases} L_2 = L_{\rm cs1} \\ C_2(k) = \frac{Z_5(k)}{s} \\ R_2 = 0 \\ U_2 = \frac{U_{\rm C2}(k-1)}{s} - L_2 I_{\rm L2}(k-1) \end{cases} \tag{15}$$

$$\begin{cases} L_3 = L_{\rm gin1} + L_{\rm g1} \\ C_3(k) = \frac{Z_6(k)}{s} \\ R_3 = R_{\rm g1} \\ U_3 = \frac{U_{\rm C3}(k-1)}{s} - L_3 I_{\rm L3}(k-1) \end{cases} \tag{16}$$

where $C_{\rm n}(k)$ is the value of capacitance at $t_{\rm k}$.

According to the equivalent circuit in Fig. 5, during time interval $t_{\rm k\text{-}1}$–$t_{\rm k}$, the relationship between crosstalk voltage $V_{\rm gs}$ and $V_{\rm in}$ can be obtained as

$$V_{\rm gs}(s) = \frac{Z_2(R_{\rm g1} + sL_{\rm g1})}{Z_1Z_3 + Z_1Z_2 + Z_2Z_3} V_{in}(s) + \frac{(R_{\rm g1} + sL_{\rm g1})(Z_1U_2 - Z_2U_1 - (Z_1 + Z_2)U_3)}{Z_1Z_3 + Z_1Z_2 + Z_2Z_3}. \tag{17}$$

The crosstalk voltage can be regarded as the full response with zero state response and zero input response as shown in (17), where $G_{\rm zs}(s)$ is the transfer function of zero state response of system and $Y_{\rm zi}(s)$ represents the zero input response

$$V_{\rm gs}(s) = G_{zs}(s)V_{in}(s) + Y_{zi}(s). \tag{18}$$

Fig. 6 shows the structure diagram of the proposed crosstalk voltage analytical model, which is used to calculate the transient value of crosstalk voltage. It mainly consists of three parts: the calculation of drain current, the calculation of common source current, and the calculation of gate–source voltage. According to

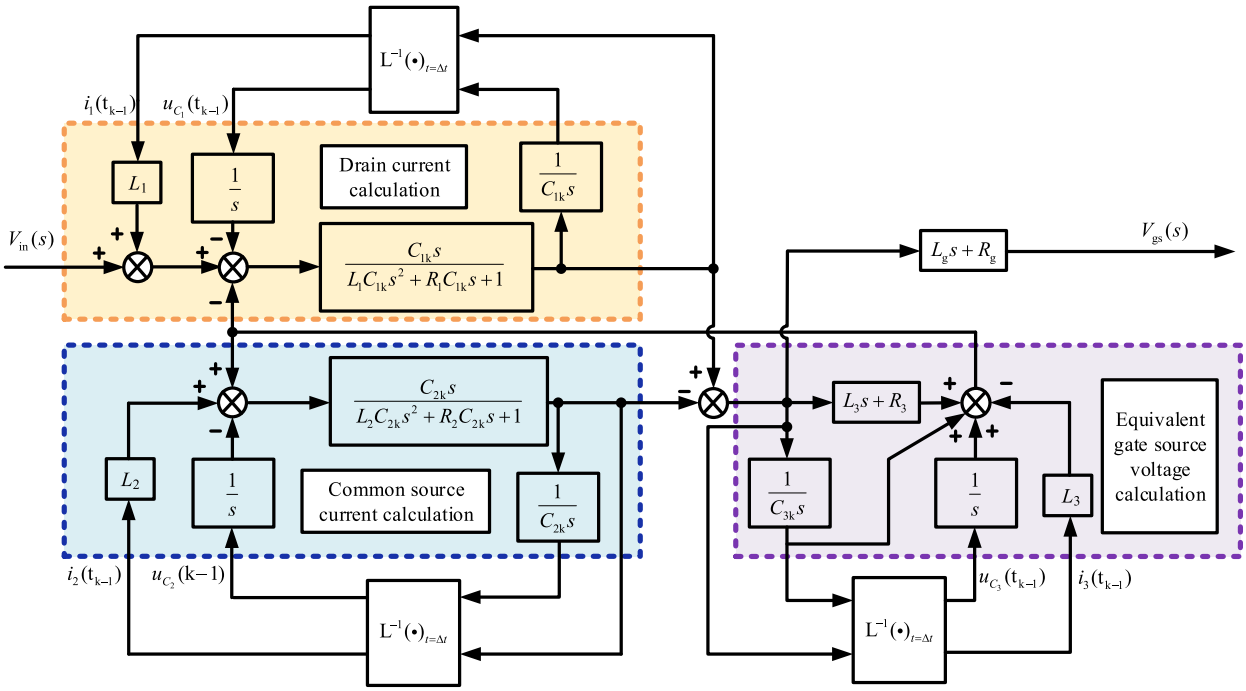

Fig. 6. Structure diagram of the proposed crosstalk voltage analytical model.

Fig. 5, the equivalent circuit of bridge-leg configuration contains six equivalent energy storage elements, including three inductive elements and three capacitive elements. Therefore, when V_{gs} is solved in time domain, the current values i_1, i_2, and i_3 of inductive elements, the voltage values u_{c1}, u_{c2}, and u_{c3} of capacitive elements need to be calculated as the initial value in the next calculation cycle. First, the instantaneous values of the applied slope excitation signals V_{in}, u_{c1}, and i_1 are substituted into branch 1 to solve $i_1(s)$, and $i_2(s)$ can be solved according to u_{c2} and i_2. Then subtract the currents of the two branches to get the current of branch 3. In the end, V_{gs} (s) can be solved according to the impedance of branch 3.

Among the device models, the fixed-parameter model, Pspice model, and full-parameter analytical model are commonly used models for the study of transient switching characteristics. The fixed-parameter model considers the parasitic elements in the device but ignores the nonlinearities, which is easy to be built, and the simulation time is short. However, the simulation results are less accurate. The Pspice model improves the simulation accuracy compared with the fixed-parameter model, and the simulation time is a little longer than the fixed-parameter model. However, the Pspice model is usually provided by the device supplier, the voltages and currents inside the device package are not convenient to be extracted. The full-parameter analytical model has the highest simulation accuracy; however, there are numerous parameters to be set in the model. It is much more complex than the proposed model and needs longer simulation time.

Compared with the previous commonly used model, the proposed model is established for studying the crosstalk. Therefore, some characteristics of GaN device are not modeled to simplify the model on the premise of guaranteeing the accuracy. The simplified method is introduced in detail in the next paragraph. Besides, the proposed model is convenient to get the inside package voltages and currents. It is helpful to monitor the actual gate–source voltage and provide guidelines for circuit optimization. Meanwhile, the damping ratio and the oscillation frequency of crosstalk voltage can be calculated easily. The attenuation characteristic of crosstalk voltage can be analyzed according to the damping ratio and the oscillation frequency. The differences in the proposed model and traditional models are listed in Table III.

TABLE III
COMPARISON OF DIFFERENT KINDS OF MODELS

Model approach	Complexity	Simulation time	Accuracy	Inside information
Fixed-parameter model	Not complex	shortest	Not accurate	Visible
Pspice model	More complex	short	More accurate	Not visible
Full-parameter analytical model	Most complex	long	Most accurate	Visible
Proposed model	Complex	shorter	More accurate	Visible

The proposed model still keeps the nonlinear gate–drain capacitance and drain–source capacitance, which affect the simulation accuracy significantly. However, the gate–source capacitance with little change rate is seen as the fixed one. The channel I–V relationship determining the static characteristics is ignored. The CtrlTR is replaced by a ramp voltage. These methods simplify the model to be a system of four state variables. Besides, the nonlinearity calculation of the system can be dealt with by employing iteration. The number of nonlinear elements in the model, the number of total parameters to be extracted, and

TABLE IV
COMPLEXITY COMPARISON OF MODELS CONSIDERING NONLINEARITY

Model approach	Nonlinear elements	Parameters to be extracted	State variables	Accuracy
Circuit model	8	28	-	More accuracy
Full-parameter analytical model	8	174	16	Most accuracy
Behavior model	6	22	-	Accuracy
Proposed model	2	16	4	More accuracy

the number of state variables in the analytical model can be used to describe the complexity of the whole model. The comparison of these aspects is shown in Table IV. In which, the circuit model, full-parameter analytical model, and behavior model are presented in [26], [29], and [32], respectively. According to Table IV, the proposed model could balance the accuracy and complexity in the crosstalk simulation.

III. INFLUENCE ANALYSIS OF DEVICE AND CIRCUIT PARAMETERS ON CROSSTALK VOLTAGE

A. Influence of Device and Circuit Parameters on Crosstalk Voltage Amplitude

The magnitude of crosstalk voltage affects the reliability of the drive system significantly. When the crosstalk voltage amplitude is higher than the threshold voltage of SyncTR, C_{gs} is charged. Since the GaN HEMT device Q_g is about one-tenth of the MOSFET device at the same power level, it is very sensitive to the crosstalk voltage. According to the previously established equivalent analytical model, the main factors affecting the crosstalk voltage of GaN devices include the rising speed of drain–source voltage, the stray inductance L_c of the power circuit, the common source inductance L_{cs} shared by the power circuit and the drive circuit, the drive resistance R_g, and the drive circuit parasitic inductance L_g. Among them, the rising speed of drain–source voltage is determined by the turn-ON speed of the CtrlTR. The faster the drain–source voltage rising speed, the greater the amplitude of the crosstalk voltage generated. However, the design and selection of the CtrlTR turn-ON speed need to consider the balance of multiple factors in practical applications.

The influence of the device and circuit parameters on the crosstalk voltage of the SyncTR is shown in Fig. 7. The contour line marked in the figure is the threshold voltage of the GaN HEMT device (GS66508B) at 1.5 V. It can be seen from Fig. 7(a) that the drive resistance has a significant influence on the amplitude. If no other suppression strategies are employed, the drive resistance needs to be less than 4 Ω. As can be seen from Fig. 7(b), with the increasing of L_g, the crosstalk voltage will also increase. However, Fig. 7(c) shows that the increase of L_c will suppress the crosstalk voltage. It is because when L_c increases, the voltage rise speed can be suppressed. In Fig. 7(d), L_{cs} has different effects on crosstalk voltage at different drain–source voltages. The increase of L_{cs} has a little effect on the amplitude of crosstalk voltage when the voltage is small, while the crosstalk

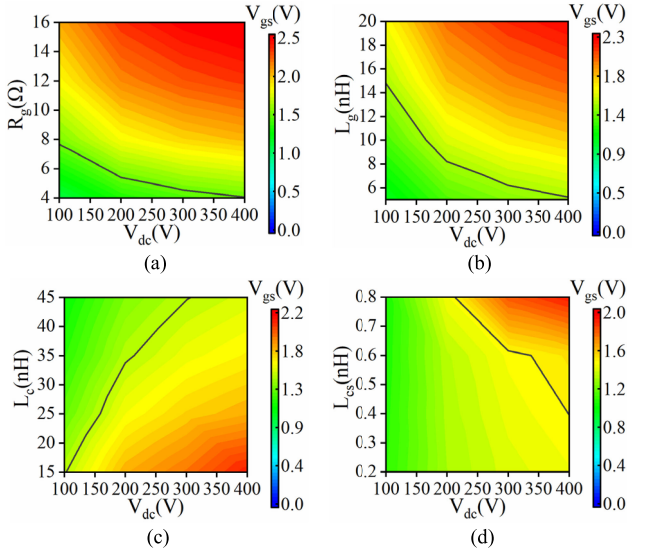

Fig. 7. Influence of different device and circuit parameters on crosstalk voltage amplitude. (a) Influence of R_g. (b) Influence of L_g. (c) Influence of L_c. (d) Influence of L_{cs}.

voltage increases with L_{cs} when voltage is high. The main reason is that the feedback capacitance decreases rapidly with the voltage increasing.

B. Influence of Device and Circuit Parameters on Crosstalk Voltage Oscillation

For the crosstalk phenomenon of SyncTR, in addition to the influence of circuit parameters on the amplitude of crosstalk voltage, the long-term oscillation of crosstalk voltage also adversely affects the drive reliability. Therefore, the situation of crosstalk voltage oscillation needs to be analyzed. The model proposed in this article is convenient for the analysis of crosstalk voltage oscillations.

When the drain–source voltage is 0 V, the pole–zero diagram of the system zero state response part transfer function is shown in Fig. 8(a). From the zoomed view in Fig. 8(b), it can be seen that the conjugate poles p_1 and $p_1{}^*$ are closer to the imaginary axis relative to other poles. It can be regarded as the dominant poles, which mainly determines the transient characteristics of the system. According to p_1 and $p_1{}^*$, the system's damping ratio ξ and the oscillation frequency f can be obtained. Both the system damping ratio and the oscillation frequency reflect the oscillation of crosstalk voltage. The effects of damping ratio and oscillation frequency are shown in Fig. 9(a)–(h), respectively.

It can be seen from Fig. 9(a) and (b) that as L_c increases, the system damping ratio and the oscillation frequency decrease, which will slow down the crosstalk voltage attenuation rate. It is not conducive to system reliability. According to Fig. 9(c), it can be found that an increase in L_{cs} causes the reduction of damping ratio, and the system's oscillation attenuation will slow down. But it has almost no effect on the system oscillation frequency according to Fig. 9(d). It can be seen from Fig. 9(e) that the effect of R_g on the damping ratio is different under different voltages. When the voltage is low, the increase of R_g will cause

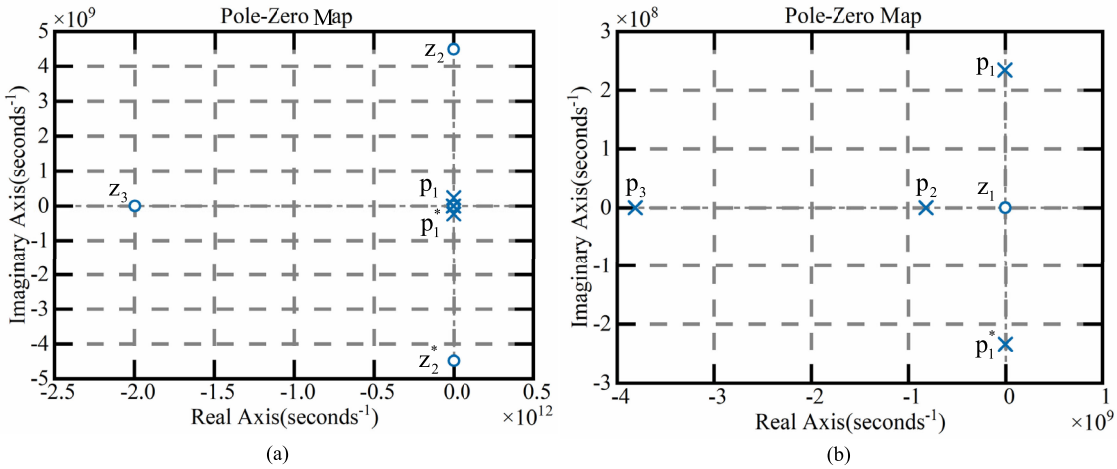

Fig. 8. Pole–zero map of $G_{zs}(s)$. (a) Pole–zero map of $G_{zs}(s)$. (b) Zoomed view of part pole–zero map.

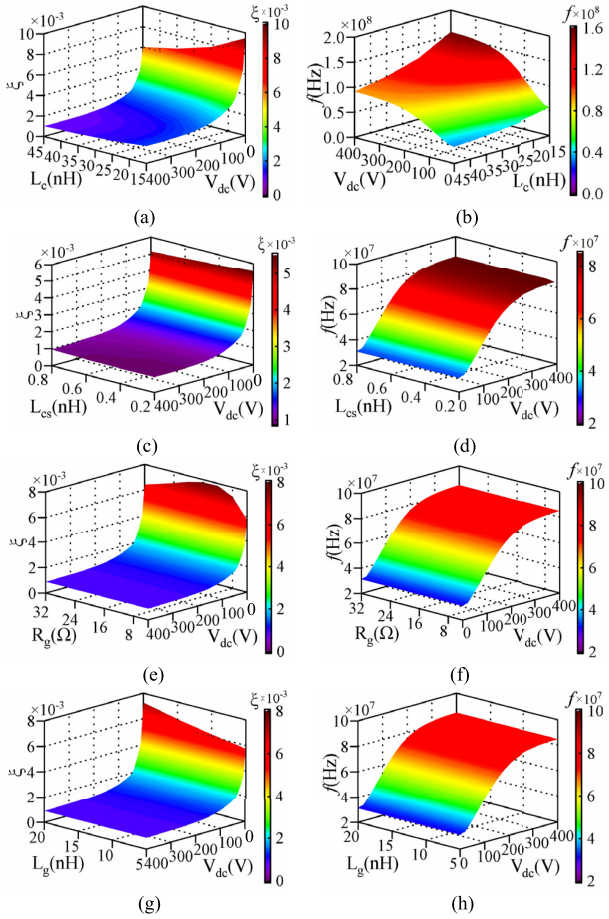

Fig. 9. Influences of device and circuit parameters on damping ratio ξ and oscillation frequency f. (a) ξ vs. L_c. (b) f vs. L_c. (c) ξ vs. L_{cs}. (d) f vs. L_{cs}. (e) ξ vs. R_g. (f) f vs. R_g. (g) ξ vs. L_g. (h) f vs. L_g.

the system attenuation speed to become faster until $R_g = 12\ \Omega$ and then the attenuation speed slow down. The inflection point is affected by other parameters. However, the effect is not obvious at high voltage. According to Fig. 9(f), R_g does not affect the

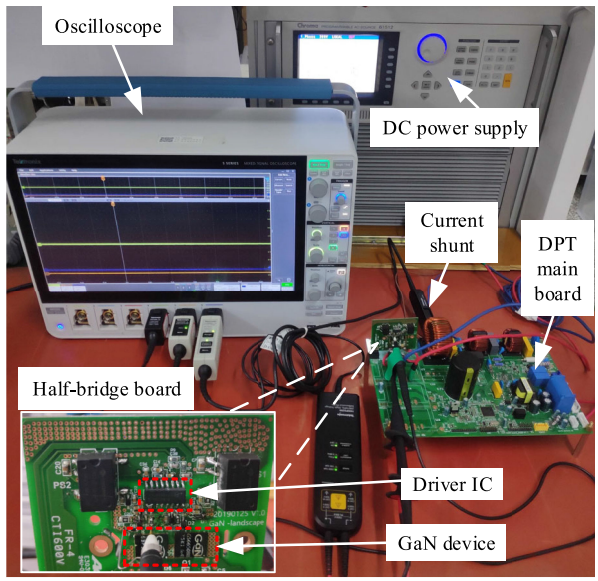

Fig. 10. Experimental platform for DPT.

system oscillation frequency. It can be seen from Fig. 9(g) and (h) that an increase in L_g will increase the system damping ratio and cause the crosstalk voltage to rapidly decrease, but L_g has little effect on the oscillation frequency.

IV. Experimental Verification

As shown in Fig. 10, the proposed bridge-leg crosstalk model of GaN HEMT with nonlinear junction capacitances is validated on a DPT platform. The switching GaN HEMTs are GS66508B (650 V GaN device produced by GaN System Inc.) with 1.5 V threshold voltage. The driver IC is Si8273, in order to protect GaN devices from crosstalk voltage, the turn-OFF voltage is set as -3 V. The V_{gs} is measured by a TPP1000 probe with 1 GHz bandwidth and the inductor current is measured using TCP0030A. The load inductance is 100 μH. The dc-link voltage is controlled by dc power supply.

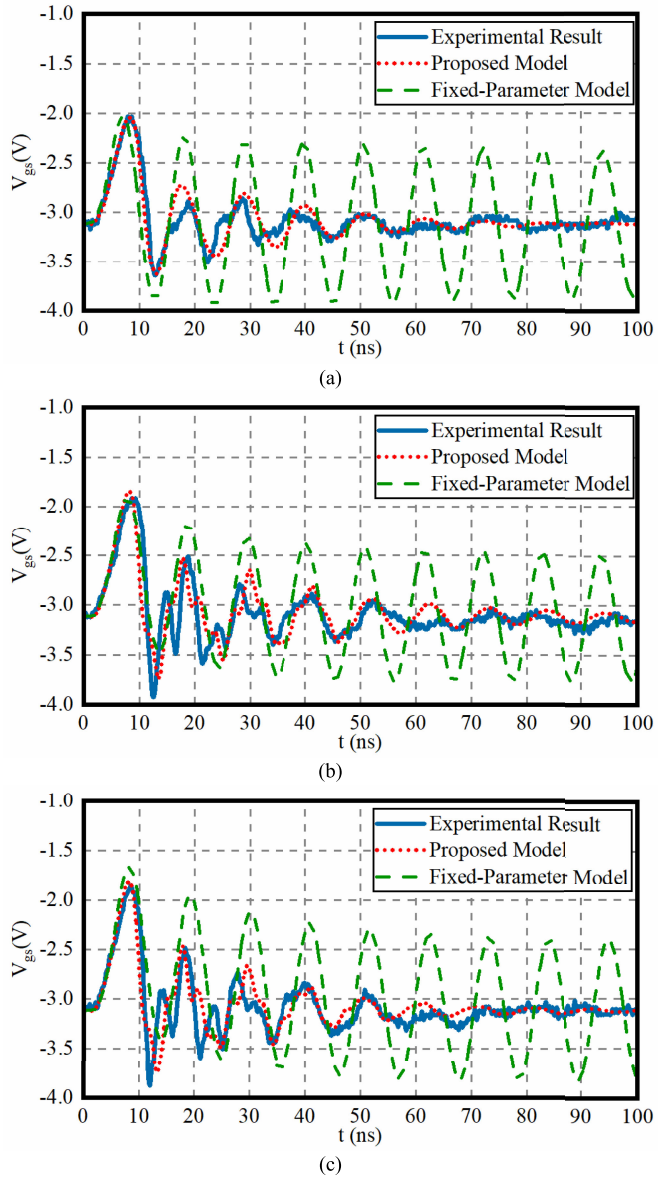

Fig. 11. Comparison of experimental and simulation waveforms of the gate–source voltage in the different dc-link voltage with circuit parameters in Table I. (a) DC-link voltage is 100 V. (b) DC-link voltage is 300 V. (c) DC-link voltage is 400 V.

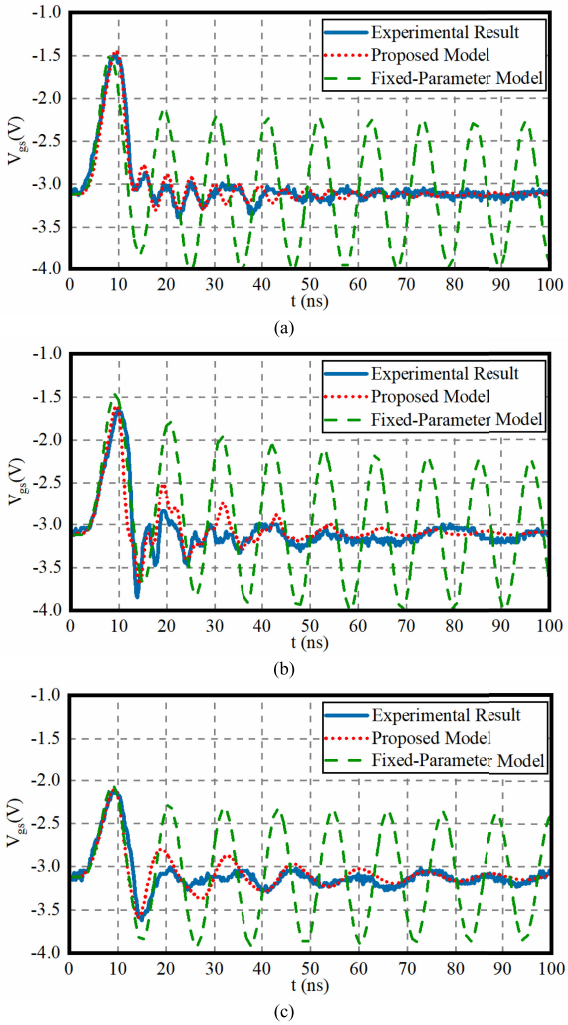

Fig. 12. Comparison of experimental and simulation waveforms of the gate–source voltage with different circuit parameters. (a) Gate resistance is 7.5 Ω. (b) Drive circuit inductance is 8 nH. (c) Power circuit inductance is 52 nH.

To verify the accuracy of the proposed crosstalk voltage model, the comparisons of fixed-parameter model, proposed nonlinear capacitances model, and experimental results are shown as Figs. 11 and 12. The values of $C_{\rm gd}$, $C_{\rm ds}$, and $C_{\rm gs}$ are 11, 64, and 250 pF, respectively, in fixed-parameter model. In three subgraphs of Fig. 11, the parameters of the device and circuit are the same, except for the dc-link voltage. In Fig. 11(a)–(c), the dc-link voltages are 100, 300, and 400 V, respectively. As can be seen that the amplitude and the oscillation frequency of the fixed-parameter model simulation results are close to the experimental results. However, the decay time is longer than that of experimental results significantly, due to the errors of junction capacitances, especially the gate–drain capacitance $C_{\rm gd}$ is only 1–2 pF, about one-sixth of the fixed-parameter model when drain–source voltage is over 50 V. The proposed model with nonlinear junction capacitances can solve this problem well.

Fig. 12 shows the simulation results of the proposed nonlinear junction capacitances model and fixed-parameter model and compares them with experimental results in different circuit parameters. In Fig. 12(a), the gate resistance is adjusted as 7.5 Ω, the dc-link voltage is 100 V, and other parameters are the same as these in Table I. Compared with Fig. 11(a), the amplitude of crosstalk voltage increases, and the oscillation attenuation time decreases, which are consistent with the theoretical analysis in this article. The proposed nonlinear junction capacitance model can also simulate this result. However, the fixed-parameter model only reflects the change in amplitude, the error on oscillation attenuation time increases instead. Fig. 12(b) shows the waveforms that the drive circuit inductance is increased to 8 nH, and the dc-link voltage is 400 V. Compared with Fig. 11(c), the amplitude increases with drive circuit inductance, and oscillation attenuation time reduces. Because of the influence of fixed junction capacitances, the amplitude of the fixed-parameter model is

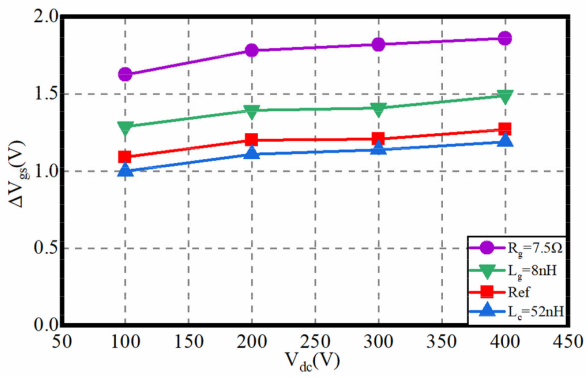

Fig. 13. Amplitude of the crosstalk voltage in the different circuit parameters.

higher than the actual value when the dc-link voltage increases. This result verifies the analysis conclusion based on Fig. 2. The influence of the power circuit inductance on the crosstalk voltage is shown in Figs. 11(a) and 12(c). Compared with Fig. 11(a), the power circuit inductance is changed to 52 nH in Fig. 12(c). With the increase of power circuit inductance, the amplitude of the crosstalk voltage reduces and the oscillation attenuation time is longer. The power circuit inductance can slow down the slope rate of drain–source voltage but harms the overvoltage during the turn OFF process. According to the simulation results in Figs. 11 and 12, the fixed-parameter model cannot exhibit the oscillation attenuation time of crosstalk voltage and the amplitude error are different under different dc-link voltages.

Fig. 13 shows the experimental results with the change in V_{gs} amplitude. The reference curve indicates the result under the gate resistance $R_g = 4\ \Omega$, the drive circuit inductance $L_g = 5$ nH, and the power circuit stray inductance $L_c = 39$ nH. When R_g increases to 7.5 Ω, the amplitude of crosstalk voltage increases. The result of $L_g = 8$ nH proves that the amplitude of crosstalk voltage increases with L_g, and the result of $L_c = 52$ nH exhibits the negative correlation between the crosstalk voltage and L_c. The influence on the amplitude of the crosstalk voltage caused by circuit parameters mentioned above is consistent with the model analysis results.

V. Conclusion

This article investigates the bridge-leg crosstalk voltage model of GaN HEMT considering junction capacitances nonlinearity. It is used to evaluate the amplitude and oscillation of crosstalk voltage in bridge circuits for guiding GaN device selection and PCB circuit design. The appropriate equivalent circuits of CtrlTR and SyncTR effectively reduce the number of parameters to be extracted, which can simplify the bridge-leg crosstalk model. Taking into account the nonlinear characteristic of junction capacitances during the drain–source voltage variation in the model is helpful to improve the simulation accuracy. Both the amplitude and oscillation of the crosstalk voltage are taken as indicators, which can judge the PCB design more comprehensively. According to the established model, optimizing the power circuit, reducing drive circuit and gate resistance are the effective methods to suppress the amplitude of crosstalk voltage. Besides, appropriate negative turn-OFF voltage could protect the device against false turn-ON. The accuracy of the model is verified through experiments with different circuit parameters. The analysis of crosstalk voltage performance is also verified through the experimental results and it can contribute to the further study of crosstalk voltage.

References

[1] E. A. Jones, F. F. Wang, and D. Costinett, "Review of commercial GaN power devices and GaN-based converter design challenges," *IEEE J. Emerg. Sel. Top. Power Electron.*, vol. 4, no. 3, pp. 707–719, Sep. 2016.

[2] W. Zhang, F. Wang, D. J. Costinett, L. M. Tolbert, and B. J. Blalock, "Investigation of gallium nitride devices in high-frequency LLC resonant converters," *IEEE Trans. Power Electron.*, vol. 32, no. 1, pp. 571–583, Jan. 2017.

[3] F. C. Lee and Q. Li, "High-frequency integrated point-of-load converters: Overview," *IEEE Trans. Power Electron.*, vol. 28, no. 9, pp. 4127–4136, Sep. 2013.

[4] R. Mitova, R. Ghosh, U. Mhaskar, D. Klikic, M. Wang, and A. Dentella, "Investigations of 600-V GaN HEMT and GaN diode for power converter applications," *IEEE Trans. Power Electron.*, vol. 29, no. 5, pp. 2441–2452, May 2014.

[5] H. A. Mantooth, M. D. Glover, and P. Shepherd, "Wide bandgap technologies and their implications on miniaturizing power electronic systems," *IEEE J. Emerg. Sel. Top. Power Electron.*, vol. 2, no. 3, pp. 374–385, Sep. 2014.

[6] X. She, A. Q. Huang, Ó. Lucía, and B. Ozpineci, "Review of silicon carbide power devices and their applications," *IEEE Trans. Ind. Electron.*, vol. 64, no. 10, pp. 8193–8205, Oct. 2017.

[7] R. Ramachandran and M. Nymand, "Experimental demonstration of a 98.8% efficient isolated DC–DC GaN converter," *IEEE Trans. Ind. Electron.*, vol. 64, no. 11, pp. 9104–9113, Nov. 2017.

[8] Q. Huang and A. Q. Huang, "Review of GaN totem-pole bridgeless PFC," *CPSS Trans. Power Electron. Appl.*, vol. 2, no. 3, pp. 187–196, Nov. 2017.

[9] M. Fernández *et al.*, "Short-circuit study in medium-voltage GaN cascodes, p-GaN HEMTs, and GaN MISHEMTs," *IEEE Trans. Ind. Electron.*, vol. 64, no. 11, pp. 9012–9022, Nov. 2017.

[10] X. Huang, W. Du, F. C. Lee, Q. Li, and W. Zhang, "Avoiding divergent oscillation of a cascode GaN device under high-current turn-off condition," *IEEE Trans. Power Electron.*, vol. 32, no. 1, pp. 593–601, Jan. 2017.

[11] Z. Liu, X. Huang, F. C. Lee, and Q. Li, "Package parasitic inductance extraction and simulation model development for the high-voltage cascode GaN HEMT," *IEEE Trans. Power Electron.*, vol. 29, no. 4, pp. 1977–1985, Apr. 2014.

[12] E. Gurpinar, F. Iannuzzo, Y. Yang, A. Castellazzi, and F. Blaabjerg, "Design of low-inductance switching power cell for GaN HEMT based inverter," *IEEE Trans. Ind. Appl.*, vol. 54, no. 2, pp. 1592–1601, Mar./Apr. 2018.

[13] A. Lemmon, M. Mazzola, J. Gafford, and C. Parker, "Instability in half-bridge circuits switched with wide band-gap transistors," *IEEE Trans. Power Electron.*, vol. 29, no. 5, pp. 2380–2392, May 2014.

[14] X. Long, W. Liang, Z. Jun, and G. Chen, "A normalized quantitative method for GaN HEMT turn-on overvoltage modeling and suppressing," *IEEE Trans. Ind. Electron.*, vol. 66, no. 4, pp. 2766–2775, Apr. 2019.

[15] K. Wang, X. Yang, L. Wang, and P. Jain, "Instability analysis and oscillation suppression of enhancement-mode GaN devices in half-bridge circuits," *IEEE Trans. Power Electron.*, vol. 33, no. 2, pp. 1585–1596, Feb. 2018.

[16] T. Wu, "Cdv/Dt induced turn-on in synchronous buck regulators," *Int. Rectifier*, El Segundo, CA, USA, Tech. Rep., 2007. [Online]. Available: http://www.irf.com/, doi: 10.1109/TPEL.2013.2268058.

[17] J. Wang and H. S.-H. Chung, "Impact of parasitic elements on the spurious triggering pulse in synchronous buck converter," *IEEE Trans. Power Electron.*, vol. 29, no. 12, pp. 6672–6685, Dec. 2014.

[18] C. Li *et al.*, "High off-state impedance gate driver of SiC MOSFETs for crosstalk voltage elimination considering common-source inductance," *IEEE Trans. Power Electron.*, vol. 35, no. 3, pp. 2999–3011, Mar. 2020.

[19] J. Wang and H. S.-H. Chung, "A novel RCD level shifter for elimination of spurious turn-on in the bridge-leg configuration," *IEEE Trans. Power Electron.*, vol. 30, no. 2, pp. 976–984, Feb. 2014.

[20] Z. Zhang, F. Wang, L. M. Tolbert, and B. J. Blalock, "Active gate driver for crosstalk suppression of SiC devices in a phase-leg configuration," *IEEE Trans. Power Electron.*, vol. 29, no. 4, pp. 1986–1997, Apr. 2013.
[21] L. Dulau, S. Pontarollo, A. Boimond, J. Garnier, N. Giraudo, and O. Terrasse, "A new gate driver integrated circuit for IGBT devices with advanced protections," *IEEE Trans. Power Electron.*, vol. 21, no. 1, pp. 38–44, Jan. 2006.
[22] M. A. H. Broadmeadow, G. F. Ledwich, and G. R. Walker, "An improved gate driver for power MOSFETs using a cascode configuration," in *Proc. 7th IET Int. Conf. Power Electron. Mach. Drives*, 2014, pp. 1–6.
[23] GS66508B Preliminary Datasheet, Rev.190502, 2019, [Online]. Available: http://www.gansystems.com/.
[24] IPx60R125P6 Datasheet, Rev. 2.0 Final, 2014, [Online]. Available: http://www.infineon.com/.
[25] R. Khanna, A. Amrhein, W. Stanchina, G. Reed, and Z. Mao, "An analytical model for evaluating the influence of device parasitics on Cdv/dt induced false turn-on in SiC MOSFETs," in *Proc. 28th Annu. IEEE Appl. Power Electron. Conf. Expo.*, 2013, pp. 518–525.
[26] R. Xie, H. Wang, G. Tang, X. Yang, and K. J. Chen, "An analytical model for false turn-on evaluation of high-voltage enhancement-mode GaN transistor in bridge-leg configuration," *IEEE Trans. Power Electron.*, vol. 32, no. 8, pp. 6416–6433, Aug. 2017.
[27] T. Zhu, F. Zhuo, F. Zhao, F. Wang, and T. Zhao, "Quantitative model-based false turn-on evaluation and suppression for cascode GaN devices in half-bridge applications," *IEEE Trans. Power Electron.*, vol. 34, no. 10, pp. 10166–10179, Oct. 2019.
[28] A. Endruschat, C. Novak, H. Gerstner, T. Heckel, C. Joffe, and M. März, "A universal SPICE field-effect transistor model applied on SiC and GaN transistors," *IEEE Trans. Power Electron.*, vol. 34, no. 9, pp. 9131–9145, Sep. 2019.
[29] H. Li, X. Zhao, W. Su, K. Sun, X. You, and T. Q. Zheng, "Nonsegmented PSpice circuit model of GaN HEMT with simulation convergence consideration," *IEEE Trans. Ind. Electron.*, vol. 64, no. 11, pp. 8992–9000, Nov. 2017.
[30] Z. Duan, T. Fan, X. Wen, and D. Zhang, "Improved SiC power MOSFET model considering nonlinear junction capacitances," *IEEE Trans. Power Electron.*, vol. 33, no. 3, pp. 2509–2517, Mar. 2018.
[31] K. Chen, Z. Zhao, L. Yuan, T. Lu, and F. He, "The impact of nonlinear junction capacitance on switching transient and its modeling for SiC MOSFET," *IEEE Trans. Electron. Devices*, vol. 62, no. 2, pp. 333–338, Feb. 2015.
[32] M. Turzynski and W. J. Kulesza, "A simplified behavioral MOSFET model based on parameters extraction for circuit simulations," *IEEE Trans. Power Electron.*, vol. 31, no. 4, pp. 3096–3105, Apr. 2016.

Binxing Li (Student Member, IEEE) received the B.S. degree in electrical engineering from the Harbin Institute of Technology, Weihai, China, in 2017. He is currently working toward the Ph.D. degree in power electronics and electrical drives with the Harbin Institute of Technology, Harbin, China.

His current research interests include permanent magnet synchronous motor drives, high efficiency ac–dc converter, and application of GaN power devices.

Gaolin Wang (Senior Member, IEEE) received the B.S., M.S., and Ph.D. degrees in electrical engineering from the Harbin Institute of Technology, Harbin, China, in 2002, 2004, and 2008, respectively.

In 2009, he joined the Department of Electrical Engineering, Harbin Institute of Technology as a Lecturer, where he has been a Full Professor of electrical engineering since 2014. From 2009 to 2012, he was a Postdoctoral Fellow with Shanghai Step Electric Corporation, Shanghai, China, where he was involved in the traction machine control for direct-drive elevators. He has authored more than 100 technical papers published in journals and conference proceedings. He is the holder of ten Chinese patents. His current major research interests include permanent magnet synchronous motor drives, high performance direct-drive for traction system, position sensorless control of ac motors, efficiency optimization control of permanent magnet synchronous motors, and digital control of power converters.

Dr. Wang serves as a Guest Associate Editor for the IEEE TRANSACTIONS ON INDUSTRIAL ELECTRONICS, and an Associate Editor for *IEEE Access*, *IET Electric Power Applications*, and *Journal of Power Electronics*.

Shaobo Liu received the B.S. and M.S. degrees in electrical engineering from the Harbin Institute of Technology, Harbin, China, in 2018 and 2020, respectively, where he is currently working toward the Ph.D. degree in power electronics and electrical drives.

His current research interests include high efficiency ac–dc converter, parameter identification technique, and application of GaN power devices.

Nannan Zhao (Member, IEEE) received the B.S. and M.S. degrees in control science and engineering, and the Ph.D. degree in electrical engineering from the Harbin Institute of Technology, Harbin, China, in 2013, 2015, and 2019, respectively.

Currently he is a Postdoctoral Fellow and a Lecturer with the School of Electrical Engineering and Automation, Harbin Institute of Technology. His current research interests include advanced control of permanent magnet synchronous motor drives and position sensor-less control of ac motors. He is currently supported by Postdoctoral Innovative Talent Support Program of China.

Guoqiang Zhang (Member, IEEE) received the B.S. degree in electrical engineering from Harbin Engineering University, Harbin, China, in 2011, and the M.S. and Ph.D. degrees in electrical engineering from the Harbin Institute of Technology, Harbin, China, in 2013 and 2017, respectively.

Since 2017, he has been with the Department of Electrical Engineering, Harbin Institute of Technology, where he is currently an Associate Professor. His current research interests include control of electrical drives, and parameter identification technique, with main focus on sensorless field-oriented control of synchronous motor drives.

Dr. Zhang currently serves as an Associate Editor for the *Journal of Power Electronics*.

Xueguang Zhang (Member, IEEE) was born in Heilongjiang Province, China, in 1981. He received the B.S., M.S., and Ph.D. degrees in electrical engineering from the Harbin Institute of Technology, Harbin, China, in 2003, 2005, and 2010, respectively.

In 2010, he joined the Department of Electrical Engineering, Harbin Institute of Technology as a Lecturer, where he has been an Associate Professor of electrical engineering since 2014. His current research interests include distributed generation and renewable energy conversion systems.

Dianguo Xu (Fellow, IEEE) received the B.S. degree in control engineering from Harbin Engineering University, Harbin, China, in 1982, and the M.S. and Ph.D. degrees in electrical engineering from the Harbin Institute of Technology (HIT), Harbin, China, in 1984 and 1989, respectively.

In 1984, he joined as an Assistant Professor with the Department of Electrical Engineering, HIT, where he has been a Professor since 1994. From 2000 to 2010, he was the Dean of School of Electrical Engineering and Automation, and is currently the Vice President of HIT. His research interests include renewable energy generation technology, power quality mitigation, sensorless vector controlled motor drives, and high performance servo system. He has authored or coauthored over 600 technical papers.

Dr. Xu is an Associate Editor for the IEEE TRANSACTIONS ON INDUSTRIAL ELECTRONICS and the IEEE JOURNAL OF EMERGING AND SELECTED TOPICS IN POWER ELECTRONICS. He curerntly serves as Chairman of IEEE Harbin Section.